Int J Thermophys (2009) 30:833–850
DOI 10.1007/s10765-009-0572-8

End Effects in the Three-Omega Method to Measure Gas Thermal Conductivity

E. Yusibani · P. L. Woodfield · M. Kohno · K. Shinzato · Y. Takata · M. Fujii

Received: 19 November 2008 / Accepted: 4 March 2009 / Published online: 2 April 2009

Abstract A two-dimensional analytical solution is derived for the three-omega method for measurement of thermal conductivity of materials with a fine wire. The analytical solution includes the wire heat capacity and the effect of heat losses from the ends of the wire. To derive the solution, finite Fourier transforms are applied in the direction parallel to the wire axis. The solution is compared with a one-dimensional solution and experimental data. It is found that heat losses from the wire ends have a significant effect on the 3ω components at low frequency and tend to be less important at high frequency. Moreover, it is shown that two-dimensional effects will be severe for nano-scale wires, even if the wire length-to-diameter ratio is very large.

Keywords Gas · Hydrogen · Nano wire probe · Three-omega · Two-dimensional analytical solution · Thermal conductivity

List of symbols

c_p	Heat capacity at constant pressure
f	Frequency
I_o	Magnitude of the oscillating current
K_0	Modified Bessel function of 0th order
K_1	Modified Bessel function of 1st order
K	Kernel function
l	Length of the wire
P_o	Time-average of power ($=I_\mathrm{o}^2 R_T/2$)

E. Yusibani (✉) · M. Kohno · Y. Takata
Department of Mechanical Engineering, Kyushu University, Fukuoka, Japan
e-mail: e-yusibani@aist.go.jp

P. L. Woodfield · K. Shinzato · M. Fujii
Research Center for Hydrogen Industrial Use and Storage, Hydrogenius, AIST, Fukuoka, Japan

r_0	Radius of the wire
r	r-coordinate
R_T	Resistance of the wire at temperature $T + T_0$
R_{0C}	Resistance of wire at 0 °C
t	Time
T	Temperature change relative to T_0
$\overline{T}_n$	Fourier transform for temperature
T_{avg}	Volume-averaged oscillation temperature component
T_0	Initial temperature of the bath (°C)
V_Y	Out-of-phase 3ω voltage component
V_X	In-phase 3ω voltage component
$V_{fg3\omega}$	3ω voltage in function generator signal
X	Magnitude of 3ω voltage of in-phase component
Y	Magnitude of 3ω voltage of out-of-phase component
z	z-coordinate

Greek symbols

α_s	Thermal diffusivity of the sample
β	Temperature coefficient of resistance $(=(\mathrm{d}R_T/\mathrm{d}T) \cdot R_{0C}^{-1})$
γ	Euler's constant (0.5772…)
λ_s	Thermal conductivity of the sample
λ_w	Thermal conductivity of the wire
ρ	Density
ω	Phase frequency $(\mathrm{rad} \cdot \mathrm{s}^{-1})$

Subscripts

avg	Average
gen	Signal generator
max	Maximum
min	Minimum
ref	Reference resistor
w	Properties of the wire

1 Introduction

The three-omega method is attractive for measuring thermal conductivity, because only a small sample is required and the experiment is relatively simple. The heating element is typically either a metallic strip adhered to (or plated onto) a solid sample [1,2] or a fine wire immersed in a fluid or powder sample [3,4]. One-dimensional analytical solutions for the 3ω voltage components are available for both of these cases [1–4]. In the case of the heated strip, potential taps are also usually included in the plated pattern far enough from the ends of the line to eliminate edge effects and thus to justify a one-dimensional analysis [1]. Cahill [1,2] derived 3ω voltage components using a one-dimensional analytical treatment for cases where the strip is attached to

the sample directly. Griesinger et al. [4] performed two-dimensional numerical simulations for a fine wire heated by a very low-frequency oscillating current (<1 Hz). Their simulations showed some agreement with their one-dimensional analytical solution for samples with thermal conductivities higher than $0.05\,\mathrm{W \cdot m^{-1} \cdot K^{-1}}$. On the other hand, for lower thermal-conductivity samples the agreement was poorer. Griesinger et al. attributed this to heat losses including the neglect of the cold end effect and neglect of the wire heat capacity in the analytical analysis. They concluded that heat loss corrections may be essential for the further development of the periodic hot wire method (viz. 3ω method), particularly in the case of a low thermal-conductivity sample.

Wang et al. [3] applied the three-omega method to measurement of nano-fluid thermal conductivities using a 17 μm diameter platinum wire, 8 mm in length. They used a one-dimensional analysis derived on the basis that the length of the wire is much greater than the radius. To validate the calibration of their apparatus, they reported a measurement of the thermal conductivity for water at 20 °C of $0.58\,\mathrm{W \cdot m^{-1} \cdot K^{-1}}$ which is within a few percent of the value recommended by the International Association for the Properties of Water and Steam (IAPWS) [5]. Wang et al. [3] also suggested that natural convection effects may be reduced by increasing the frequency of the oscillating current.

In most of the studies done until now, the three-omega method has been applied to determination of the thermal conductivity or heat capacity of solids, thin films, powders, and liquids. Through the use of a high vacuum and a different theoretical formulation, three-omega methods are also available to measure the properties of the heating element itself. Lu et al. [6] and Yi et al. [7] derived one-dimensional solutions to determine specific heat and thermal conductivity of wire specimens and nanotube bundles. Application of the three-omega method to the measurement of gas phase properties is still difficult. One important reason for this is that we do not obtain a straight line when we plot the in-phase 3ω voltage component against the logarithm of the frequency. In a recent study, we showed that this non-linearity is due to the fact that the effect of the wire heat capacity becomes large for gas samples [8]. This is inconvenient because in Cahill's experiment, the slope of the straight line is used directly to determine the thermal conductivity of the sample [1]. Therefore, to derive thermal conductivity of a gas by the three-omega method, we need to employ some kind of curve-fitting procedure or we need to use an extremely fine wire (diameter <1 μm). Curve fitting procedures have been used in three-omega methods for measuring the properties of the wire [6].

One-dimensional solutions that include a consideration of wire properties can be found in Ref. [3], however we are unaware of any published solution for the two-dimensional case. The solution we derive in the present article could be the basis for a more generalized curve-fitting procedure to determine thermal conductivity for situations where both the wire heat capacity and end effects are important. It is suitable for application to a small sample with a short wire, similar to that used in the transient short-hot-wire method developed by Fujii et al. [9]. Our own present application of interest is measurement of the thermal conductivity of hydrogen gas from atmospheric pressure to 100 MPa. The three-omega method is attractive since a small pressure vessel is in keeping with safety regulations.

Based on these motivations, a two-dimensional analytical solution is derived for the three-omega voltage components including wire heat capacity and end effects. By the use of finite Fourier transforms, the two-dimensional problem is reduced to a set of one-dimensional characteristic problems. The form of each one-dimensional equation is somewhat similar to that of our previous study [8], so that finally the derivation can proceed in a similar manner. The importance of the end-effect correction we suppose is greater at low frequencies, small wire aspect ratios, and for high thermal-diffusivity samples. At low frequencies, in-phase and out-of-phase voltage components are larger than at high frequencies, and thus they are easier to measure accurately. Therefore the present correction can be tested experimentally and may become valuable if it can extend the range of valid data to include more of the low-frequency region. Finally, the derived analytical solution is compared with three-omega voltage components measured from a fine platinum wire in air at atmospheric pressure.

2 Two-Dimensional Physical Model

The two-dimensional physical model is illustrated in Fig. 1. The partial differential equation for heat conduction in cylindrical coordinates is given by

$$\frac{1}{r}\frac{\partial T}{\partial r} + \frac{\partial^2 T}{\partial r^2} + \frac{\partial^2 T}{\partial z^2} = \frac{1}{\alpha_s}\left(\frac{\partial T}{\partial t}\right) \tag{1}$$

and the boundary condition at the wire and the sample interface, $r = r_0$, along the wire is described by Eq. 2. Equation 3 shows the temperature boundary condition for the

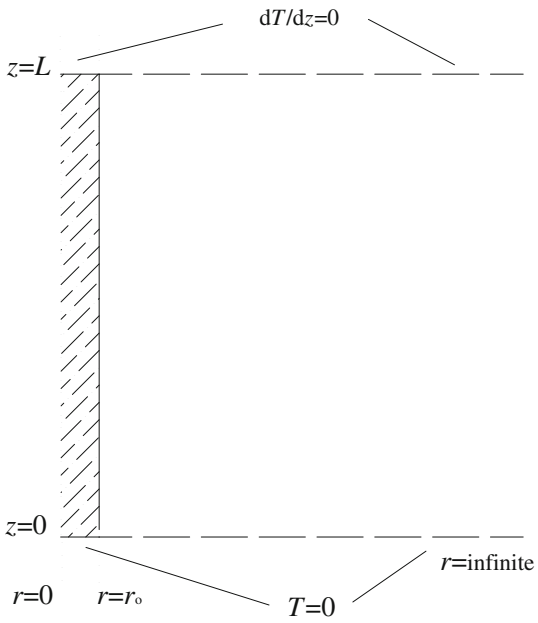

Fig. 1 Domain and boundary conditions for two-dimensional analytical solution

sample in which the effect of the cell wall is neglected by assuming that frequencies are sufficiently high so that the penetration of the thermal oscillations does not reach the wall.

$$-2\pi r_0 \lambda_s \frac{\partial T}{\partial r}\Big|_{r=r_0} = \frac{P}{l} + \pi r_0^2 \lambda_w \frac{\partial^2 T}{\partial z^2}|_{r=r_0} - \pi r_0^2 \left(\rho c_p\right)_w \frac{\partial T}{\partial t}\Big|_{r=r_0} \tag{2}$$

$$T|_{r\to\infty} = 0 \tag{3}$$

$$T|_{z=0} = \frac{\partial T}{\partial z}\Big|_{z=L} = 0 \tag{4}$$

In Eq. 2 we have neglected the radial temperature gradient in the wire but not the axial temperature gradient. The range of the variable z in Eqs. 1 and 2 is $(0 \le z \le L)$ where L is a half of the wire length. The wire is heated by an oscillating current, $I_o \cos(\omega t)$. In Eq. 2, $P = R_T(I_o \cos(\omega t))^2$ is the power supplied to the total wire length, $l = 2L$. Since the resistance changes slightly with temperature, for evaluating the power in an experiment, R_T should be taken to be the time-averaged resistance of the wire. For simplicity, in the present simulations we take R_T to be the electrical resistance of the wire at the bath temperature. Rather than including an initial condition, we consider only the 'steady oscillation' part of the solution. Equation 4 provides the necessary z-boundary conditions for both Eqs. 1 and 2. The partial derivatives of $T(r, z, t)$, with respect to the variable z can be eliminated from the problem by applying Fourier transforms in the z direction. The problem then reduces to a one-dimensional problem. After solving the one-dimensional problem and applying the inverse transform, the average magnitude of the oscillating temperature over the wire length is used for calculating the three-omega voltage components. The final results for the in-phase (V_X) and the out-of-phase (V_Y) three-omega voltage components are given in Eq. 5. See the Appendix for the details of the derivation.

$$\begin{aligned} V_X &= X\cos 3\omega t = \frac{I_o^3 R_{0C} R_T \beta}{\pi l^3} \sum_{n=1}^{\infty} \frac{1}{m_n^2} \left(\frac{(BD - AC)}{(C^2 + D^2)} \right) \cos 3\omega t \\ V_Y &= Y\sin 3\omega t = \frac{I_o^3 R_{0C} R_T \beta}{\pi l^3} \sum_{n=1}^{\infty} \frac{1}{m_n^2} \left(\frac{(AD + BC)}{(C^2 + D^2)} \right) \sin 3\omega t \end{aligned} \tag{5}$$

where A, B, C, D, and m_n are defined in Eq. 6a, 6b, 6c, 6d, and 6e.

$$A = \ln\left(\frac{r_0}{2} \left(\frac{4\omega^2}{\alpha_s^2} + m_n^4 \right)^{1/4} \right) + \gamma \tag{6a}$$

$$B = \frac{1}{2} \tan^{-1}\left(\frac{2\omega}{\alpha_s m_n^2} \right) \tag{6b}$$

$$C = \lambda_s - A\frac{r_0^2\lambda_w m_n^2}{2} + Br_0^2\left(\rho c_p\right)_w \omega \tag{6c}$$

$$D = r_0^2\left(\rho c_p\right)_w \omega A + B\frac{r_0^2\lambda_w m_n^2}{2} \tag{6d}$$

$$m_n = \pi\left(\frac{2n-1}{l}\right) \tag{6e}$$

3 Experiment

To test the present analytical solution, an experiment was conducted with air at atmospheric pressure. Figure 2 shows the experimental setup. A 10 µm platinum wire of length 15.6 mm is enclosed in a stainless steel cylindrical vessel with an inside diameter of 30 mm and height of 47 mm. The wire is spot-welded onto 1.5 mm diameter platinum lead terminals. The oscillating current is generated by a signal generator WF1974 (NF Corporation) which has an internal resistance of 50 Ω. The three-omega voltage components were extracted using a lock-in-amp, DSP 7265 (Signal Recovery). The reference signal input to the lock-in-amp was the voltage drop across a 25 Ω reference resistor connected in series with the platinum wire in the thermal conductivity cell. The cell was immersed in a thermostatic bath to ensure stable thermal conditions. As an additional check, the lock-in-amp shown in Fig. 2 was replaced with a 2-channel, 24-bit high-speed analog/digital converter, PXI-5922 (National Instruments) and the experiment was repeated. Fourier transforms were used to extract the three-omega components from the voltage signal measured by the A/D board

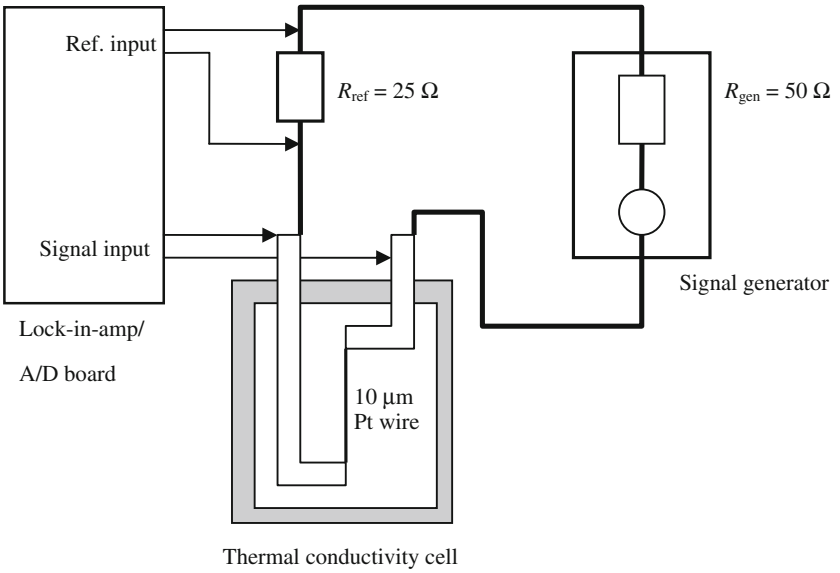

Fig. 2 Experimental setup

converter. To compensate for the fact that the function generator produces an alternating voltage rather than a pure alternating current, the 3ω voltage components in Eq. 5 are multiplied by the factor $(R_{\text{gen}} + R_{\text{ref}})/(R_T + R_{\text{gen}} + R_{\text{ref}})$ prior to comparison with the experimental data. The derivation for this correction factor is given in a previous study [8] where the key assumption is that the function generator can be modeled as a perfect oscillating voltage source ($V_{\text{fg}3\omega} = 0$) in series with its internal resistance as illustrated in Fig. 2. It is worth mentioning that this correction factor is not needed in the circuit of Cahill [1] or in bridge circuits which make use of the A-B function of the lock-in-amp [3]. Moreover, the effect of imperfections in the signal generator ($V_{\text{fg}3\omega} \neq 0$) can also be reduced through the use of bridge circuits or by direct measurement of the 3ω components in the voltage across the reference resistor in Fig. 2 [8].

4 Results

4.1 Comparison with Experiment

To validate the applicability of the present analysis to gases, the analytical solution was compared with experimental data for air at a temperature of 20 °C. The range of frequencies was from 5 Hz to 1 kHz, with 1.55 V for the signal generator voltage. For this setting with the circuit in Fig. 2, the magnitude of the oscillating current I_o is about 16 mA. The aspect ratio (l/D) of the wire is 1560. Figure 3 shows the present analytical result compared with the experimental data. The two-dimensional analytical solution (solid-line) gives a lower estimation than the one-dimensional analytical solution (dashed-line) due to the heat losses at the ends of the wire. The one-dimensional solution, which is derived in the previous study [8], includes the heat capacity of the wire. At low frequency, the in-phase 3ω components (X) measured by the lock-in-amp

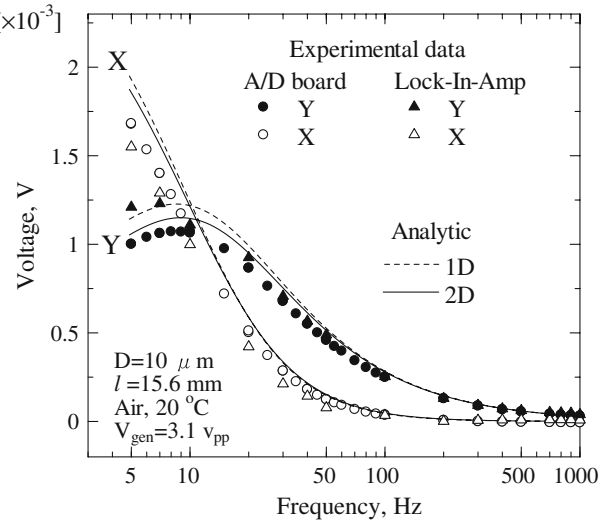

Fig. 3 Experimental data compared with the analytical solution ($I_o \approx 16$ mA)

(open triangles) are a little lower than those measured by the A/D board (open circles). On the other hand, the out-of-phase components (Y) (filled symbols) measured by the lock-in-amp are generally a little larger than the corresponding values measured by the A/D board. Nevertheless, the agreement between the experimental data collected by the A/D board and the present solution is within about 10 % of the magnitudes of the 3ω voltage components at frequencies less than about 50 Hz. Moreover, the 2D solution is in better agreement with the experimental data than the 1D solution.

Although not clear in Fig. 3, the A/D board data appeared to have much less noise than the lock-in-amp data. The output from the lock-in-amp did not stay constant with time but oscillated about the values shown in Fig. 3. Therefore we consider that the A/D board data is more reliable. We expect that the lock-in-amp data may be improved by subtracting the 1ω signal component prior to analysis with the instrument [1]. Also, as mentioned above, in the case of a real signal generator ($V_{\mathrm{fg}3\omega} \neq 0$) the experimental result of the present study will be in error by an amount corresponding to the 3ω spurious signal in the source [8].

The difference between the calculation and experiment may be attributed to uncertainties in the length and diameter of the platinum wire, imperfections in the generated signal and to heat losses by natural convection. Some of these effects could be compensated for by calibration of the wire in a fluid of known thermal conductivity. It is also worth mentioning here that $I_{\mathrm{o}} = 16$ mA for air with the present geometry corresponds to an average wire temperature rise of around 9 K. The increase in the thermal conductivity of air due to this temperature rise is less than 3 %. Using a smaller current with the present circuit arrangement is desirable but was found to result in a lower quality 3ω-voltage signal as explained in a previous study [8]. In spite of these difficulties, the experimental results shown in Fig. 3 indicate that the present solution is applicable to gases.

4.2 End Effects in Relation to Frequency, Sample Properties, and Aspect Ratio

Further simulations were done for hydrogen, water, and toluene at 20 °C as shown in Figs. 4, 5, and 6. The circuit is the same as that shown in Fig. 2. Also, the geometry and electrical current are similar to those used in the experiment to allow comparison with the results for air shown in Fig. 3. For the simulations, a platinum wire is used with a 10 µm diameter and a 15 mm length. Thus the aspect ratio is 1500. The function generator voltage in the simulations in Figs. 4, 5, and 6 was 2.4 V peak to peak, which for the circuit in Fig. 2 gives $I_{\mathrm{o}} \approx 12$ mA. In all of the simulations, the results from Eq. 5 are multiplied by the factor $(R_{\mathrm{gen}} + R_{\mathrm{ref}})/(R_T + R_{\mathrm{gen}} + R_{\mathrm{ref}})$ to be consistent with the circuit used in the experiment.

It may be observed from Figs. 3, 4, 5, and 6 that the difference between the one- and two-dimensional solutions is greater at lower frequencies. Thus the present study confirms that an end-effect correction is needed at low frequencies and is less important at high frequencies. Based on the simulations in Figs. 5 and 6, the end effect correction has a contribution at low frequency even for water and toluene. For the water case, the discrepancy between 1D and 2D simulations reaches 0.95 % and 2 % for X and Y components, respectively. Therefore we should not neglect this effect if we want

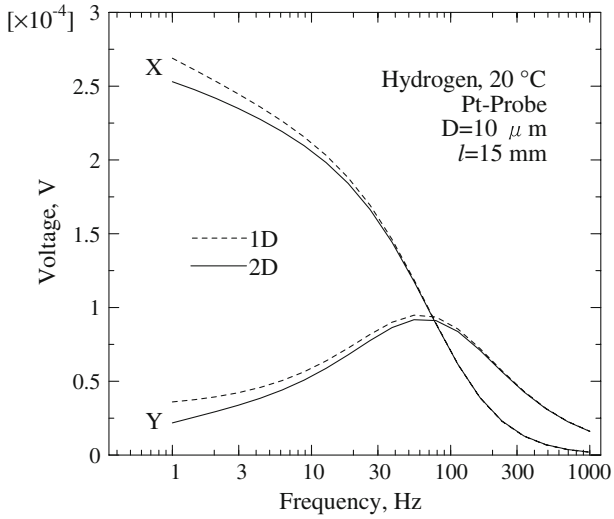

Fig. 4 Simulated 3ω voltage components for hydrogen gas at atmospheric pressure

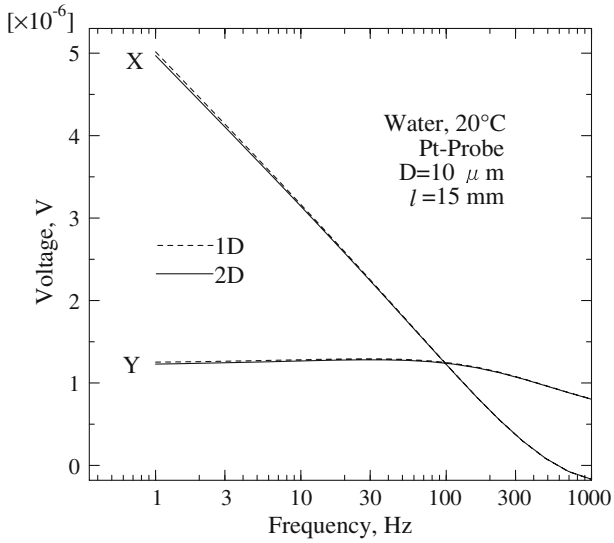

Fig. 5 Simulated 3ω voltage components for liquid water

measurements of high accuracy using a short-hot-wire thermal conductivity cell. For the gaseous cases shown in Figs. 3 and 4, the end effect is greater than that for liquids due to the high thermal diffusivities. Especially for the hydrogen case (Fig. 4), up to 100 Hz, the end effect is very important. It is also worth noting that for the same current ($I_o \approx 12$ mA), the 3ω voltages in the case of water (Fig. 5) are more than an order of magnitude smaller than those for hydrogen (Fig. 4) and toluene (Fig. 6). This is related to the higher thermal conductivity of water.

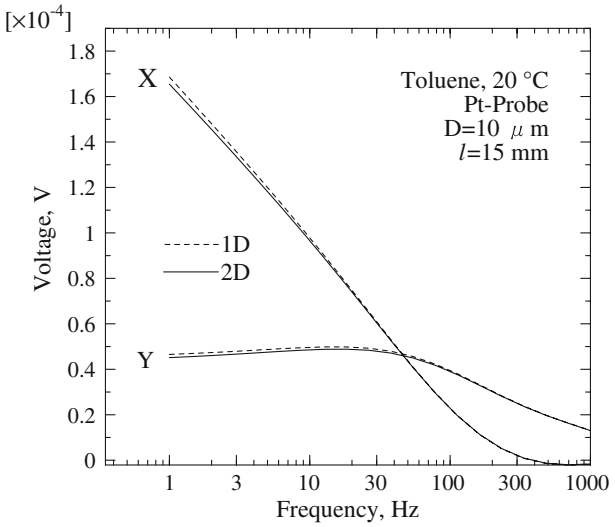

Fig. 6 Simulated 3ω voltage components for toluene

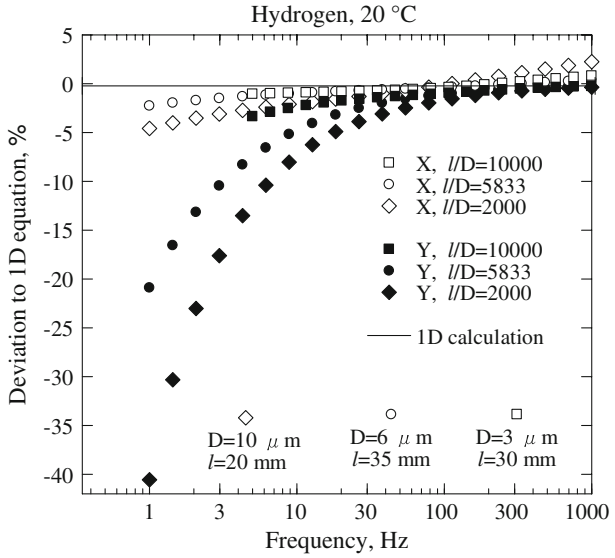

Fig. 7 Deviation of two-dimensional analytical solution from one-dimensional solution for 3ω voltage components

We also investigated the end effect correction in relation to the aspect ratio of the wire. Figure 7 shows the percentage deviation of the 2D solution from the 1D solution for different aspect ratios of the wire. Generally, increasing the aspect ratio leads to an improvement in the accuracy of the 1D approximation as should be expected. For many of the results in Fig. 7, the percentage deviation for the out-of-phase component (Y) is significantly larger than that of the in-phase component (X). The important

conclusion from Fig. 7 is that for aspect ratios even as high as 5800, the end effect is still not negligible, particularly for frequencies less than about 30 Hz. In this example, the discrepancy is up to 2 % for the X-component and much greater for the Y-component. For an aspect ratio as much as 10000, the deviation in the X-component is similar to that of the aspect ratio of 5800 but the deviation of the Y-component is smaller. Another interesting feature of Fig. 7 is that for frequencies greater than about 100 Hz, the in-phase component is slightly larger in the case of the 2D analytical solution in comparison with the 1D solution so that the deviation becomes positive. It is a little difficult to offer a physical explanation for this, but if low frequencies are included in the experiment, its significance may not be high since X tends to zero at high frequencies (e.g., Fig. 4).

4.3 End Effects for Nano-Wire Thermal-Conductivity Cells

In our previous study, we proposed that through the use of a nano-scale diameter wire it may be possible to design an experiment where the effect of the wire heat capacity was negligible in a low-density gas. Thus the thermal conductivity of the gas sample could be determined via the slope of the in-phase 3ω voltage component plotted against the logarithm of the frequency. Therefore it is interesting to investigate two-dimensional effects for such a fine wire using our present solution. Figure 8 shows calculations for three different nano-wire designs. The diameters are 50 nm and 100 nm and the lengths are chosen to be 10 μm, 110 μm, and 500 μm, respectively. For the wire 110 μm in length, the aspect ratio is about 2000. The dashed lines show one-dimensional simulations while the solid lines show the present solution. Surprisingly, at low frequencies, the difference between one-dimensional and two-dimensional calculations is very large. As in our previous study, the one-dimensional results show

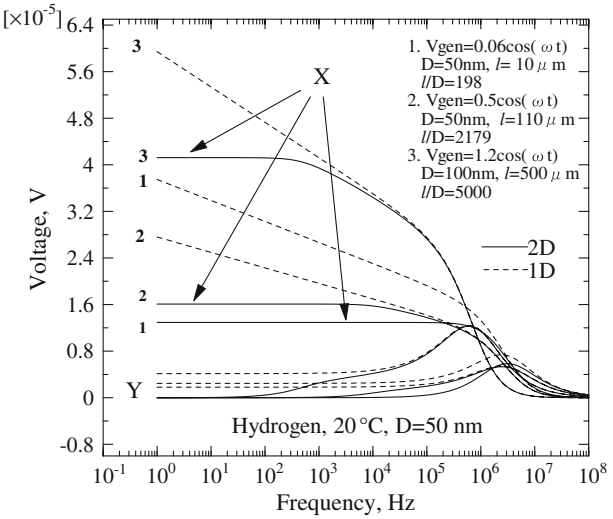

Fig. 8 Simulated 3ω voltage components for hydrogen for the case of a nano-wire

constant values for Y and a linear curve against the logarithm of frequency over a wide range of frequencies for X. In contrast, at low frequencies in the two-dimensional calculations, the out-of-phase component, Y tends to zero while the in-phase component, X, takes on a constant value. Thus end effects are severe for all three cases considered. If we compare the results in Fig. 8 with those of Figs. 4 and 7 for aspect ratios of 1500 and 2000, we find that for a similar aspect ratio, the difference between 1D and 2D solutions is much larger for the nano-wire. Thus in Fig. 8 we find that in spite of the promising results from the 1D simulations, due to end effects, a nano-wire will fail to produce a linear curve in hydrogen gas at atmospheric pressure even for an aspect ratio as large as 5000.

Figure 9 shows a nano-wire simulation for liquid water. In contrast to the hydrogen case (Fig. 8), a linear region exists in the frequency range from 10^4 to 10^6 Hz. The difference between Figs. 8 and 9 can be explained in terms of the differences in thermal diffusivity of hydrogen and water. In the case of water, the thermal diffusivity is several orders of magnitude lower so that the thermal penetration of the oscillation into the fluid surrounding the wire is much smaller. Therefore, in the case of water a longer section of the wire behaves like the one-dimensional situation. If the frequency of the oscillation is lower, then the penetration into the surrounding fluid becomes greater and the boundary condition at the wire ends is felt over a larger proportion of the wire. This phenomenon is evident by comparing the low- and high-frequency results in Figs. 8 and 9. In the low-frequency regions of Fig. 8 where X is constant, the thermal penetration is so large that the entire wire length is influenced by the boundary conditions at the ends. Therefore based on this study we can say that there are two parameters which influence the importance of the end effect correction. They are the aspect ratio (l/D) and the ratio of the wire length to the penetration depth of the oscillation into the sample surrounding the wire.

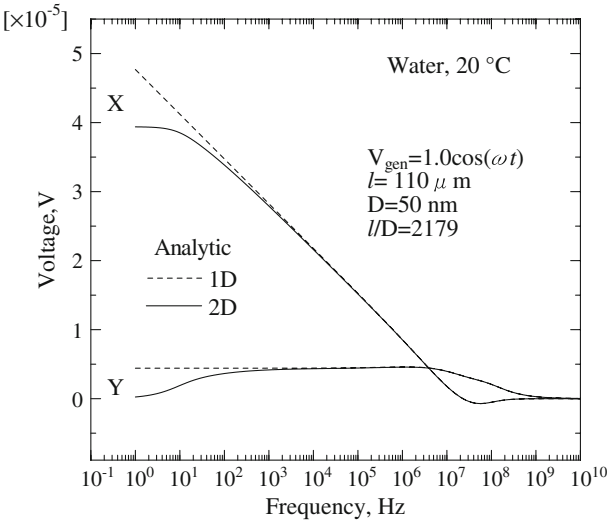

Fig. 9 Simulated 3ω voltage components for liquid water in the case of a nano-wire

5 The Importance of the Thermal Penetration Depth

The thermal penetration depth is usually defined as a multiple of the square root of the thermal diffusivity divided by the square root of the frequency. Here we take the penetration depth to be given by Eq. 7. This definition is similar to that used by Cahill [1] which is derived from a one-dimension model.

$$\delta_{\text{penetration depth}} = \sqrt{\frac{\alpha_s}{2\omega}} \tag{7}$$

In the one-dimensional analysis, the penetration depth must be sufficiently larger than the radius of the wire for validity of the truncated series approximations to the Bessel functions K_0 and K_1 [1]. This should also apply in the present solution, since similar approximations for the Bessel functions were employed in our derivation (see Appendix, Eq. A10). In addition, for Eq. 3 to be valid, the penetration depth must be smaller than the radius of the thermal conductivity cell. If we wish to neglect end effects, the restriction must be even tighter, as indicated above in Sect. 4.3. From Fig. 9, at a frequency of 10^3 Hz, the ratio $l/\delta_{\text{penetration depth}}$ is approximately 33. Thus the present simulation results suggest that the length of the wire divided by the penetration depth should be at least more than about 30. Therefore tentatively, we suggest Eq. 8 as a guide for the estimating maximum allowable penetration depth for neglecting end effects.

$$\frac{l}{\delta_{\text{penetration depth}}} \geq 30 \tag{8}$$

For convenience, Eq. 8 can be rearranged to give an estimate of the minimum frequency for which neglecting end effects may be considered valid.

$$f_{\min} = \frac{30^2 \alpha_s}{4\pi l^2} \tag{9}$$

Using Eq. 9, the minimum frequency for case 3($l/D = 5000$) in Fig. 7 is $f_{\min} = 45000$ Hz. Since this frequency is beyond the straight section of the 1D curve, Eq. 9 is consistent with the conclusions in Sect. 4.3.

Concerning the lower limit to the penetration depth, it can be observed in Fig. 9 that the in-phase component, X becomes negative at a frequency of around 2×10^7 Hz. For this frequency, the penetration depth is about 24 nm. Since this is less than the radius of the wire, the limit to the validity of the approximations for K_0 and K_1 has been exceeded. The same problem appears in Fig. 5 at around 350 Hz to 1000 Hz. At $f = 350$ Hz the penetration depth, $\delta_{\text{penetration depth}} = 5.7$ μm which again is less than the diameter of the wire itself (10 μm). A simple criterion for deciding the maximum frequency, $f_{\max}$, permitted by the present analysis is

$$\delta_{\text{penetration depth}} \geq D \tag{10}$$

Based on Eq. 10, we should limit the frequency measurement in Fig. 5 to $f_{\max} = 110\,\text{Hz}$, where the penetration depth, $\delta_{\text{penetration depth}} = 10.2\,\mu\text{m}$, to obtain a valid result. For the same wire in air due to the larger thermal diffusivity, the upper limit to the frequency is as much as $f_{\max} = 10^5\,\text{Hz}$ (for validity of the approximations used for the Bessel functions). However, practically, the influence of the gas properties on the signal at such a high frequency may be negligible compared with the effect of the wire properties. Therefore, it should be emphasized that Eq. 10 is not a criterion for neglecting the properties of the wire. To obtain results where the high-frequency signal is influenced significantly by the properties of the fluid then a comparison of the heat capacity of the sample within one penetration depth, ($\delta_{\text{penetration depth}}$) from the wire surface, with the heat capacity of the wire may be useful. Further discussion of the effect of the wire heat capacity with respect to the sample properties can be found in Ref. [8].

6 Conclusion

A two-dimensional analytical solution for application of the 3ω method to measurement of gas phase thermal conductivity has been derived. It includes the effects of heat losses at the ends of the wire and the heat capacity of the wire. Simulations of a wire 10 μm in diameter and about 15 mm in length show reasonable agreement with experimental data for air at atmospheric pressure. For this particular design, end effects should not be neglected from the calculation if we wish to make an accurate measurement of gas thermal conductivity.

The aspect ratio of the wire (l/D) is not the only parameter required to justify neglecting end effects. End effects are less important at high frequencies and less important for low thermal diffusivity samples. We also must consider the ratio of the wire length to the thermal penetration depth of the oscillations into the sample itself. This effect is particularly severe for nano-scale wires. The maximum applicable frequency of the present solution is also related to the thermal penetration depth of the oscillations. If the penetration depth is less than the diameter of the wire, the present analysis becomes invalid.

Based on this present study, we can conclude that to have a direct measurement of the thermal conductivity of hydrogen gas at atmospheric pressure by the gradient of the in-phase 3ω voltage component versus the logarithm of the frequency is impossible. Thus we need another method. The present two-dimensional formulation in conjunction with a curve-fitting procedure is a likely candidate for measurement of thermal conductivities of low-density gases by the 3ω method.

Acknowledgments This research has been conducted as a part of the "Fundamental Research Project on Advanced Hydrogen Science" funded by the New Energy and Industrial Technology Development Organization (NEDO).

Appendix. Derivation of the 2D Analytical Solution

The partial derivatives with respect to the variable z, in Eqs. 1 and 2 can be eliminated from the problem by applying Fourier transforms in the z direction. The finite Fourier

transform $\overline{T}(r,t)$ of the temperature function $T(r,z,t)$ with respect to the variable z can be defined as [10]

$$\overline{T}_n(r,t) = \int_0^L K(n,z)T(r,z,t)\mathrm{d}z \tag{A1}$$

with the inversion

$$T(r,z,t) = \sum_{n=1}^{\infty} K(n,z)\overline{T}_n(r,t) \tag{A2}$$

The kernel function appropriate for the boundary conditions specified by Eq. 4 is

$$K(n,z) = \sqrt{\frac{2}{L}}\sin(m_n z);\ m_n = \frac{(2n-1)}{L}\frac{\pi}{2};\ n = 1,2,3\ldots;\ L = l/2 \tag{A3}$$

The finite Fourier transform of Eq. 1 yields

$$\frac{1}{r}\frac{\partial \overline{T}_n}{\partial r} + \frac{\partial^2 \overline{T}_n}{\partial r^2} - m_n^2 \overline{T}_n - \frac{1}{\alpha_\mathrm{s}}\frac{\partial \overline{T}_n}{\partial t} = 0 \tag{A4}$$

Equation 2 becomes

$$-\lambda_\mathrm{s}\frac{\partial \overline{T}_n}{\partial r}|_{r=r_0} = \sqrt{\frac{2}{L}}\frac{P}{2\pi m_n r_0 l} - \frac{r_0\lambda_\mathrm{w}m_n^2}{2}\overline{T}_n|_{r=r_0} - \frac{r_0\left(\rho c_\mathrm{p}\right)_\mathrm{w}}{2}\frac{\partial \overline{T}_n}{\partial t}|_{r=r_0} \tag{A5}$$

Since we are only interested in the oscillating part of the solution, we can replace P in Eq. A5 with $P_\mathrm{o}\cos(2\omega t)$ where $P_\mathrm{o} = I_\mathrm{o}^2 R_T/2$. Moreover, since we are considering only the steady oscillation, we can eliminate t by replacing $\overline{T}_n$ in Eqs. A4 and A5 with $\overline{u}(r)e^{i2\omega t}$ and $\cos(2\omega t)$ with $e^{i2\omega t}$. We are then only interested in the real part of the solution to the ordinary differential equation:

$$\overline{T}_n = \mathrm{REAL}\left(\overline{u}(r)\mathrm{e}^{i2\omega t}\right) \tag{A6}$$

Equation A4 becomes

$$\frac{1}{r}\frac{\mathrm{d}u}{\mathrm{d}r} + \frac{\mathrm{d}^2 u}{\mathrm{d}r^2} - ik^2 u = 0 \tag{A7}$$

where

$$k = \left(\frac{2\omega - i\alpha_\mathrm{s}m_n^2}{\alpha_\mathrm{s}}\right)^{1/2}$$

Equation A5 becomes

$$-\lambda_s \frac{d\overline{u}}{dr}|_{r=r_0} = \sqrt{\frac{2}{L}} \frac{P_o}{2\pi m_n r_0 l} - \left(\frac{r_0 \lambda_w m_n^2}{2} + ir \left(\rho c_p\right)_w \omega \right) \overline{u}|_{r=r_0} \tag{A8}$$

The general solution to Eq. (A7) in terms of Bessel functions is

$$\overline{u} = Q_1 I_o(kri^{1/2}) + Q K_0(kri^{1/2})$$

When $r \to \infty$, $I_o(kri^{1/2}) \to \infty$, therefore $Q_1 = 0$ then

$$\overline{u} = Q K_0(kri^{1/2})$$

Applying Eq. A8 to find Q, we obtain

$$\overline{u} = \left(\sqrt{\frac{2}{L}} \frac{P_o}{2\pi m_n l} \right) \frac{K_0\left(kri^{1/2}\right)}{\left(\lambda_s k r_0 i^{1/2} K_1\left(kr_0 i^{1/2}\right) + \left(ir_0^2 \left(\rho c_p\right)_w \omega + \frac{r_0^2 \lambda_w m_n^2}{2} \right) K_0\left(kr_0 i^{1/2}\right) \right)} \tag{A9}$$

We now make use of the following approximations for the Bessel functions.

$$K_1(kr_0 i^{1/2}) = \frac{1}{kr_0 i^{1/2}} + \cdots \tag{A10a}$$

$$K_0\left(\left(\frac{2\omega - i\alpha_s m_n^2}{\alpha_s} \right)^{1/2} r_0 i^{1/2} \right) = -\left(\ln\left(\frac{r_0}{2} \left(\frac{i2\omega}{\alpha_s} + m_n^2 \right)^{1/2} \right) + \gamma - \cdots \right) \tag{A10b}$$

Equation A10b can be rewritten as

$$K_0\left(\left(\frac{2\omega - i\alpha_s m_n^2}{\alpha_s} \right)^{1/2} r_0 i^{1/2} \right) = -\left(\ln\left(\frac{r_0}{2} \left(\frac{4\omega^2}{\alpha_s^2} + m_n^4 \right)^{1/4} \right) + \frac{i\varphi}{2} + \gamma - \cdots \right)$$

where

$$\varphi = \tan^{-1}\left(\frac{2\omega}{\alpha_s m_n^2} \right)$$

Substituting into Eq. A9 and evaluating at $r = r_0$, we have

$$\overline{u} = \sqrt{\frac{2}{L}} \frac{P_o}{2\pi m_n l} \frac{-(A + iB)}{(C - iD)} \tag{A11}$$

where

$$A = \ln\left(\frac{r_0}{2}\left(\frac{4\omega^2}{\alpha_s^2} + m_n^4\right)^{1/4}\right) + \gamma$$

$$B = \frac{1}{2}\tan^{-1}\left(\frac{2\omega}{\alpha_s m_n^2}\right)$$

$$C = \lambda_s - A\frac{r_0^2\lambda_w m_n^2}{2} + Br_0^2\left(\rho c_p\right)_w\omega$$

$$D = r_0^2\left(\rho c_p\right)_w\omega A + B\frac{r_0^2\lambda_w m_n^2}{2}$$

The complex number can be removed from the denominator of Eq. A10 using

$$\left(\frac{1}{C - iD}\right)\left(\frac{C + iD}{C + iD}\right) = \left(\frac{C + iD}{C^2 + D^2}\right)$$

then

$$\overline{u} = \sqrt{\frac{2}{L}}\frac{P_o}{2\pi m_n l(C^2 + D^2)}[(BD - AC) - i(AD + BC)]$$

Using Eq. A6, we obtain

$$\overline{T}_n = \sqrt{\frac{2}{L}}\frac{P_o(BD - AC)}{2\pi m_n l(C^2 + D^2)}\cos 2\omega t + \sqrt{\frac{2}{L}}\frac{P_o(AD + BC)}{2\pi m_n l(C^2 + D^2)}\sin 2\omega t$$

Applying the inverse Fourier transform gives the steady oscillation component of the temperature.

$$T = \sum_{n=1}^{\infty} K(n, z)\left(\sqrt{\frac{2}{L}}\frac{P_o(BD - AC)}{2\pi m_n l(C^2 + D^2)}\right)\cos 2\omega t + \sum_{n=1}^{\infty} K(n, z)\left(\sqrt{\frac{2}{L}}\frac{P_o(AD + BC)}{2\pi m_n l(C^2 + D^2)}\right)\sin 2\omega t$$

Integrating to find the average oscillating temperature over the length of the wire gives

$$T_{avg} = \frac{4P_o}{\pi l^3}\sum_{n=1}^{\infty}\frac{1}{m_n^2}\left(\frac{(BD - AC)}{(C^2 + D^2)}\right)\cos 2\omega t + \frac{4P_o}{\pi l^3}\sum_{n=1}^{\infty}\frac{1}{m_n^2}\left(\frac{(AD + BC)}{(C^2 + D^2)}\right)\sin 2\omega t$$

To determine the voltage, we make use of the temperature resistance relationship for the wire

$$R_T = R_{0C}(1 + \beta(T_0 + T)) \tag{A12}$$

Multiplying the resistance by $I_o \cos \omega t$ and substituting $P_o = I_o^2 R_T/2$, we can obtain 3ω voltage components as follows

$$V_X = \frac{I_o^3 R_{0C} R_T \beta}{\pi l^3} \sum_{n=1}^{\infty} \frac{1}{m_n^2} \left(\frac{(BD - AC)}{(C^2 + D^2)} \right) \cos 3\omega t$$
$$V_Y = \frac{I_o^3 R_{0C} R_T \beta}{\pi l^3} \sum_{n=1}^{\infty} \frac{1}{m_n^2} \left(\frac{(AD + BC)}{(C^2 + D^2)} \right) \sin 3\omega t \quad \text{(A13)}$$

References

1. D.G. Cahill, Rev. Sci. Instrum. **61**, 802 (1990)
2. D.G. Cahill, Phys. Rev. B **50**(9), 6077 (1994)
3. Z.L. Wang, D.W. Tang, S. Liu, X.H. Zheng, A. Araki, Int. J. Thermophys. **28**, 1255 (2007)
4. A. Griesinger, W. Heidemann, E. Hahne, Int. Commun. Heat Mass Transfer, **26**, 451 (1999)
5. IAPWS (2008) Revised Release on the IAPS Formulation 1985 for the Thermal Conductivity of Ordinary Water Substance, http://www.iapws.org
6. L. Lu, W. Yi, D.L. Zhang, Rev. Sci. Instrum. **72**, 2996 (2001)
7. W. Yi, L. Lu, Z. Dian-lin, Z.W. Pan, S.S. Xie, Phys. Rev. B **59**, R9015 (1999)
8. E. Yusibani, P.L. Woodfield, M. Fujii, K. Shinzato, X. Zhang, Y. Takata, (Int. J. Thermophys. (2009), doi:10.1007/s10765-009-0563-09
9. M. Fujii, X. Zhang, N. Imaishi, S. Fujiwara, T. Sakamoto, Int. J. Thermophys. **18**, 327 (1997)
10. S. Kakac, Y. Yener, *Heat Conduction*, 2nd edn. (Hemisphere Pub. Corp, Washington, DC, 1985), p. 267